

# Field-Free Programmable Spin Logics via Chirality-Reversible Spin–Orbit Torque Switching

Xiao Wang, Caihua Wan, Wenjie Kong, Xuan Zhang, Yaowen Xing, Chi Fang, Bingshan Tao, Wenlong Yang, Li Huang, Hao Wu, Muhammad Irfan, and Xiufeng Han\*

Spin–orbit torque (SOT)-induced magnetization switching exhibits chirality (clockwise or counterclockwise), which offers the prospect of programmable spin-logic devices integrating nonvolatile spintronic memory cells with logic functions. Chirality is usually fixed by an applied or effective magnetic field in reported studies. Herein, utilizing an in-plane magnetic layer that is also switchable by SOT, the chirality of a perpendicular magnetic layer that is exchange-coupled with the in-plane layer can be reversed in a purely electrical way. In a single Hall bar device designed from this multilayer structure, three logic gates including AND, NAND, and NOT are reconfigured, which opens a gateway toward practical programmable spin-logic devices.

Spin logic based on spin–orbit torque (SOT) mechanism,<sup>[1–3]</sup> which utilizes spin Hall effect to switch magnetization for Boolean logic operations, has expressed its potential of constructing logic-in-memory computer architectures with high computing capability and low power dissipation.<sup>[4,5]</sup> As one characteristic of SOT switching, switching chirality of  $M$  versus  $I$  hysteresis loops (clockwise or counterclockwise) could be reversible<sup>[6–11]</sup> and further endow the corresponding spin-logic devices with programmability, versatility, and high integration.<sup>[12,13]</sup> However, the chirality is determined by the direction of an indispensable and symmetry-breaking field which is usually applied by an external field,<sup>[6–11,14,15]</sup> wedged structures,<sup>[16–19]</sup> or exchange bias/coupling effect<sup>[20–26]</sup> and is thus difficult to be reversibly controlled by electrical manners. Interestingly, Cai et al.<sup>[27]</sup> have shown the chirality can be electrically reversed with aid of a ferroelectric substrate. However, the controllable chirality by pure electrical manner on mainstream silicon substrates has not been realized yet. Here, we have fabricated a  $\text{SiO}_2/\text{Pt}/\text{Co}/\text{Ru}/\text{Co}/\text{Pt}$  stacked structure with crossed anisotropy in which the bottom Co layer exhibits perpendicular magnetic anisotropy, the top Co layer exhibits in-plane magnetic anisotropy, and the spacer Ru mediates interlayer exchange coupling (IEC) between them. We have

confirmed in this structure that both Co layers could be switched independently without any applied magnetic field via SOT. Meanwhile, the switching chirality of the Co layer with perpendicular anisotropy could be reversed freely by controlling the direction of the Co layer with in-plane anisotropy. Using this unique switching performance of the crossed anisotropic structure, a spin-logic device could be utilized to program AND, NAND, and NOT gates at zero magnetic field, which might advance the development of practical spin-logic devices compatible with sophisticated complementary metal oxide

semiconductor (CMOS) and magnetic random access memory technology. Besides, realization of both field-free switching of perpendicular magnet and field-free control of its switching chirality might also guide to invention of more functional memories such as four-state memory in the near future.

A structure with stacking arrangement  $\text{SiO}_2/\text{Pt}(5)/\text{Co}(0.4)/\text{Ru}(1.4)/\text{Co}(1.2)/\text{Pt}(5)$  nm were optimized to observe the crossed anisotropic magnetic configuration, where numbers in brackets were nominal thicknesses. In this stacking sequence, the bottom and top Co layers had perpendicular and in-plane anisotropy, respectively, while they were interlayer-exchange-coupled via a Ru spacer. An easy axis (EA) along the  $y$ -axis was induced by a 300 Oe in-plane field during the deposition process (Figure 1b).  $M$ – $H$  curves showed both in-plane and out-of-plane remanence due to the crossed magnetic anisotropy. Antiferromagnetic nature of the coupling effect could be inferred from reversible switching chirality in the same  $H_y$  direction (Figure 1c–e) and abnormal field-dependence of Hall resistance  $R_{xy}$ , as discussed in Sections SA and SB (Supporting Information).

For a single perpendicular Co layer, chirality can be determined by the direction of an effective field  $H_{\text{eff}}$ .<sup>[7,23]</sup> Switching behaviors of our samples with the crossed anisotropy became more versatile: the chirality could be convertible between clockwise and counterclockwise via only changing the magnitude of  $H_y$  due to an antiferromagnetic IEC field  $H_{\text{IEC}}$  (Figure 1c). The bottom perpendicular Co layer experienced both  $H_y$  and  $H_{\text{IEC}}$ ,  $H_{\text{eff}} = H_y + H_{\text{IEC}}$ , where  $H_{\text{IEC}}$  had opposite directions to the magnetization of the top in-plane Co layer. The  $H_{\text{eff}}$  direction was thus dominated by  $H_y$  as it was large enough. Instead, it was determined by  $H_{\text{IEC}}$  as  $|H_y|$  became smaller than  $|H_{\text{IEC}}|$ . Therefore, the chirality underwent a reversal as  $H_{\text{eff}} = 0$ , which indicated  $|H_{\text{IEC}}| \approx 1.8$  kOe. Due to large thicknesses and dominated transport properties of Pt layers, we estimated upper

X. Wang, Dr. C. Wan, W. Kong, Dr. X. Zhang, Y. Xing, C. Fang, Dr. B. Tao, W. Yang, L. Huang, Dr. H. Wu, M. Irfan, Prof. X. F. Han  
Beijing National Laboratory for Condensed Matter Physics  
Institute of Physics  
University of Chinese Academy of Sciences  
Chinese Academy of Sciences  
Beijing 100190, China  
E-mail: xfhan@iphy.ac.cn

DOI: 10.1002/adma.201801318

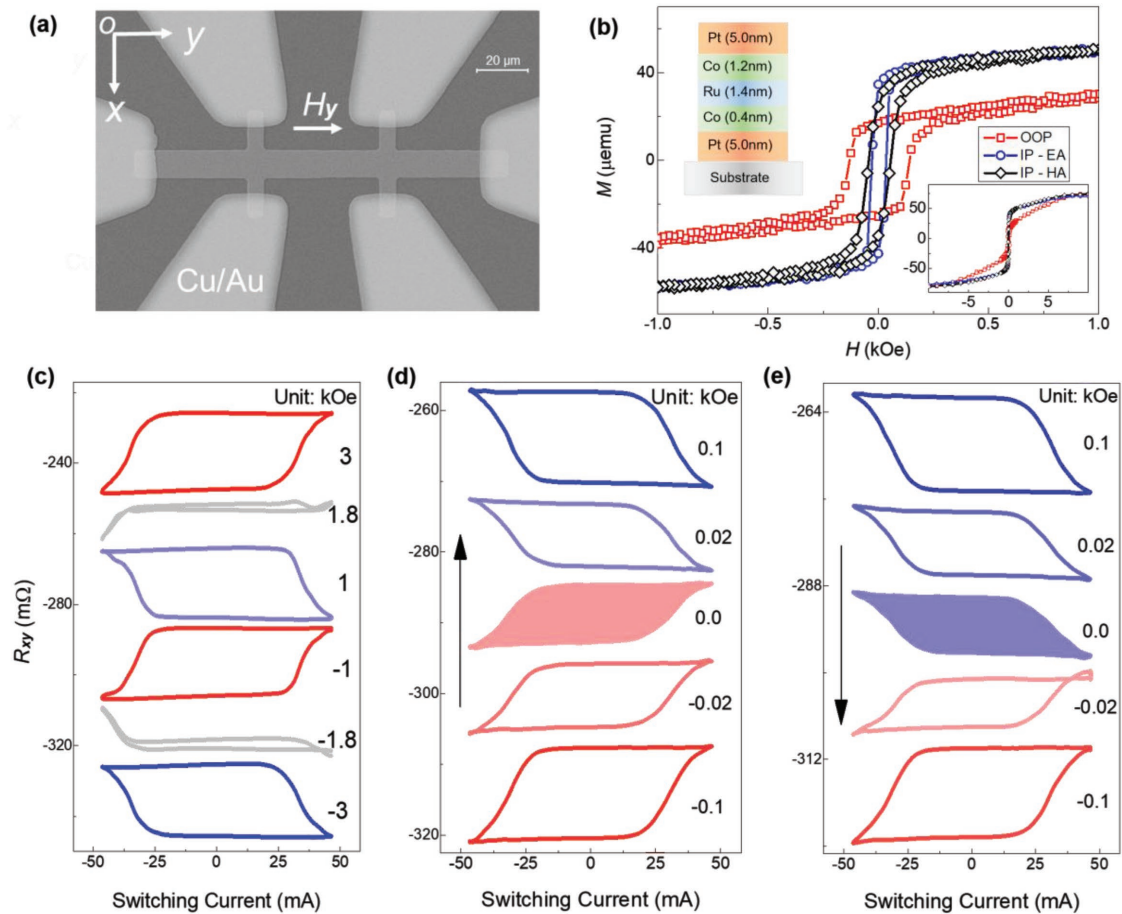


**Figure 1.** Hall bar structure of devices and their magnetic and switching behaviors. a) Scanning electron microscopy of a six-leg Hall device. b) In-plane and out-of-plane  $M$ - $H$  hysteresis of blanket film. Insets show stack structure and full  $M$ - $H$  loops at large fields. c-e) OOP, IP, EA, and HA are short for out-of-plane, in-plane, easy axis, and hard axis,  $R_{xy}$  as a function of switching current ( $I_y$ ) at various applied fields. The arrows in (d) and (e) indicate history of applying  $H_y$ .

limit of the critical current density in Pt by supposing all the current flowing through the Pt layers. Thus, the critical density in our case was around  $1.9 \times 10^7 \text{ A cm}^{-2}$  for  $|H_y| = 1 \text{ kOe}$ .

More importantly, field-free SOT switching was also experienced (Figure 1d,e), providing a strong evidence for the presence of IEC. This characteristic brought about another advantage for application: switching chirality at zero field became reversible by controlling magnetic state of the in-plane Co layer, clockwise for  $m_y^{\text{top}} > 0$  and counterclockwise for  $m_y^{\text{top}} < 0$ . Fukami<sup>[20]</sup> and Lau<sup>[24]</sup> have applied exchange bias/coupling to realize field-free switching. In both cases, exchange bias was used either to exert  $H_{\text{eff}}$  to a perpendicular layer or stabilize an in-plane magnetization layer. Thus, chirality could only be reversed by changing direction of exchange bias, which requires high-temperature annealing. Qiu<sup>[28]</sup> showed feasibility of changing chirality by interface treatment but a symmetry-breaking field was still needed. Although field-free switching and controllable switching chirality has also been demonstrated with the aid of ferroelectric substrates, this property has not been realized on silicon.<sup>[27]</sup> Here, we introduced a switchable in-plane layer that provided symmetry-breaking field via IEC. Furthermore, magnetization of the top Co layer ( $m_y^{\text{top}}$ ) with in-plane anisotropy could even

be switchable by a preset current along the  $x$ -axis ( $I_x$ ) besides the external  $H_y$  (Figure 2b).

In the above switching measurement (Figure 1c-e), current along the  $y$ -axis ( $I_y$ ) was applied. Polarization of spin current ( $\sigma // j \times z$ ) induced by spin Hall effect was thus along the  $x$ -axis, orthogonal to EA of the bottom perpendicular layer. Due to coupling with the top in-plane layer or presence of  $H_{\text{IEC}}$ , the perpendicular layer could be switched by  $I_y$ , as reported before.<sup>[21,23]</sup> Meanwhile,  $\sigma$  was also orthogonal to EA of the in-plane layer which was already along the  $y$ -axis. According to Fukami,<sup>[14]</sup> it is also possible for  $\sigma$  to switch  $m_y^{\text{top}}$  if  $H_{\text{IEC}}$  experienced by the in-plane layer with large perpendicular component. Here, owing to larger anisotropy energy of the top Co layer, only the bottom perpendicular layer was switchable in Mode I (Figure 2a). (Detailed derivation is attached in Section SC, Supporting Information.)

When  $I_x$  was applied (Figure 2b),  $\sigma$  was along the  $y$ -axis and then parallel to EA of the in-plane layer, making this layer switchable.<sup>[14,29,30]</sup> Besides,  $I_x$  was not parallel to  $H_{\text{IEC}}$ , making the perpendicular layer unswitchable. In Mode II (Figure 2b), only the in-plane layer became switchable. Thus, we could independently switch both perpendicular and in-plane layers by SOT without any applied magnetic fields in Mode I and II, respectively.

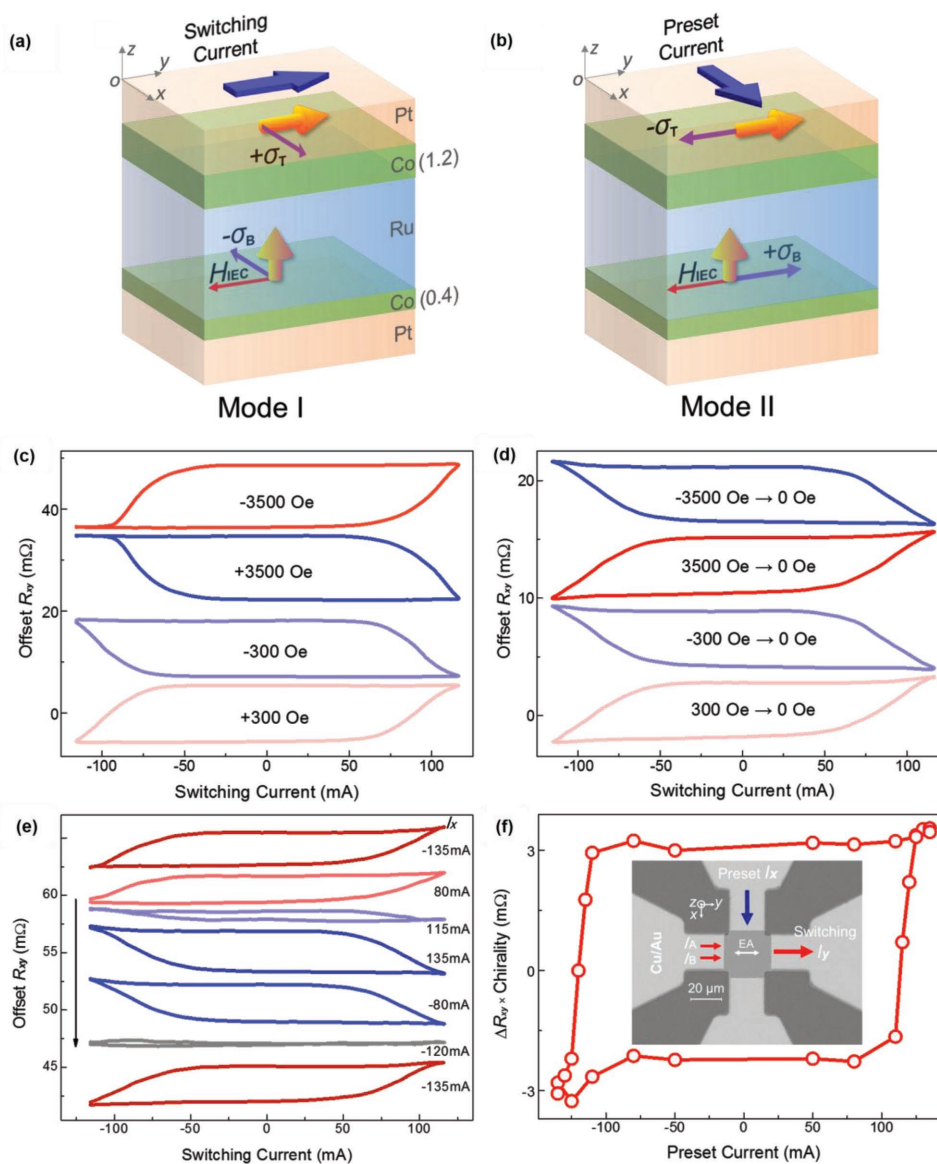


**Figure 2.** Schematic diagrams of switching Mode I and II, and manipulation of SC in the new four-leg Hall device. a,b) For Mode I and II, respectively.  $H_{IEC}$  and  $\sigma$  stand for interlayer exchange coupling field and spin–orbit torque, respectively. Switching (preset) current is parallel (normal) to the EA of the in-plane layer. The yellow arrows show the magnetization directions. c)  $R_{xy}$  as a function of  $I_y$  measured at various applied field. d) Field-free SOT switching. They were measured at zero field (outside of magnet). Applied field before field-free measurement was marked. e) Manipulation of switching chirality utilizing a preset current  $I_x$ . After excitation by different preset currents, the switching behaviors of the perpendicular layer in Mode I were tracked. The arrow indicates measurement history. f) Extracted switching behaviors as a function of the preset current.  $\Delta R_{xy} \times$  chirality characterizes both switching degree and chirality.

Another Hall bar with 20  $\mu\text{m}$  width was fabricated (Figure 2f inset) to examine Modes I and II. First, SOT switching in Mode I was reproduced in the new Hall bar (Figure 2c,d): (i) chirality underwent a reversal as only increasing magnitude of  $H_y$  and (ii) field-free switching depended on magnetizing history of the in-plane layer. In this case, the magnetization switching behavior is very similar to that shown in Figure 1c–e. Critical current density increased to  $3.3 \times 10^7 \text{ A cm}^{-2}$  in the new Hall bar due to shunting effect of wider legs.

After that, SOT-switching of in-plane layer by a preset current  $I_x$  in Mode II was achieved (Figure 2e). In this case,  $I_x$  with duration of 10 ms was first applied to “preset” magnetization

of the in-plane layer. Then  $I_x$  was shut down and  $I_y$  was applied to switch the perpendicular layer as in Mode I. From chirality of the perpendicular layer in Mode I, the preset state of the in-plane layer could be inferred:  $m_y^{\text{top}} > 0$  and  $m_y^{\text{top}} < 0$  as the chirality switched clockwise and counterclockwise, respectively. Controllability of the chirality via  $I_x$  can be easily understood from Figure 2e. For example, after applying  $I_x$  of +135 (–135) mA, the chirality in Mode I became clockwise (counterclockwise). Then the magnetization of the in-plane Co layer could be inferred along the positive (negative)  $y$ -axis. By this method, we attained the critical current density to switch the in-plane layer as shown in Figure 2f. This figure summarized

switching chirality of the perpendicular layer after different  $I_x$  excitation where  $\Delta R_{xy}$  was the difference of  $R_{xy}$  between spin-up and spin-down states at zero  $I_y$  and clockwise or counterclockwise chirality was defined as +1 or -1, respectively. The critical current density about  $4.6 \times 10^7$  A cm<sup>-2</sup> was estimated in Mode II. It is worth stressing that all the operations in Figure 2e,f and Figure 3 are demonstrated without any applied field by taking devices out of magnet. In this sense, beyond the work of Lau<sup>[23]</sup> where the in-plane layer has no access to SOT and thus unswitchable, this work provided a more versatile and electrical way to control field-free SOT-switching.

Remarkably, stability of the perpendicular (in-plane) layer was protected by symmetry requirements for SOT-switching in Mode II (Mode I). These restrictions intrinsically guaranteed safety, nonvolatility, and independency of data stored in both layers, which inspired and motivated us to design programmable spin-logic devices based on reversibility of the chirality and field-free operation.

It is worth noting that logic-in-memory architectures are regarded as an effective solution to the famous and daunting memory wall problem, a bottleneck caused by limited memory bandwidth and speed mismatch between processor and memory.<sup>[31,32]</sup> One feasible and promising way to realize the architecture is developing logic functionality in emerging non-volatile memories such as magnetic random access memory. However, a scientific challenge for the architecture still lies on searching for ideal physical systems which could be swiftly switched between different nonvolatile states and in which the switching between the states could be flexibly controlled. It is more favorable that the above switching and its control could both be executed by electric manners. Although still in infancy stage, our crossed anisotropic structure operational by SOTs inherently satisfied all the above requirements, which encouraged us to build a prototype spin-logic device.

The Hall bar structure of a spin-logic device is shown in the inset of Figure 2f. Two currents  $I_A$  and  $I_B$  as inputs were applied along the  $y$ -axis. Input values of 1 and 0 were represented by  $I_{A/B}$  values of -55 and 0 mA, respectively. Output C was characterized by  $m_z^{\text{top}}$  of the perpendicular layer or anomalous Hall resistance  $R_{xy}$  of the device. Spin-up and spin-down states denoted Output 1 and 0, respectively. In practice, as displayed by dashed lines in Figure 3, Output 1 and 0 were identified by  $R_{xy} \geq 14$  m $\Omega$  and  $R_{xy} < 14$  m $\Omega$ , respectively. Preset  $I_x$  of  $\pm 135$  mA was only used to control the direction of the in-plane layer, the switching chirality of the perpendicular layer and then define the functionality of a spin logic gate. It was switched OFF during subsequent logic operations. Besides a preset process, our spin-logic device needed another reset step to a proper initialization state as refs. [12,13,33] and final operation step to perform Boolean logics. Figure 3 presents three logic operations accomplished in a single device by utilizing different preset current  $I_x$ .

For AND gate (Figure 3a),  $I_x$  of +135 mA was first applied to align the in-plane layer along the + $y$ -axis and preset switching chirality of the perpendicular layer clockwise (Figure 2e). A critical current  $I_C$  of about 90 mA along the  $y$ -axis was then necessary to switch the perpendicular layer. Before logic operation, the perpendicular layer of a device was initially reset to spin-down state by  $I_A = I_B = 55$  mA. In the final logic operation, if

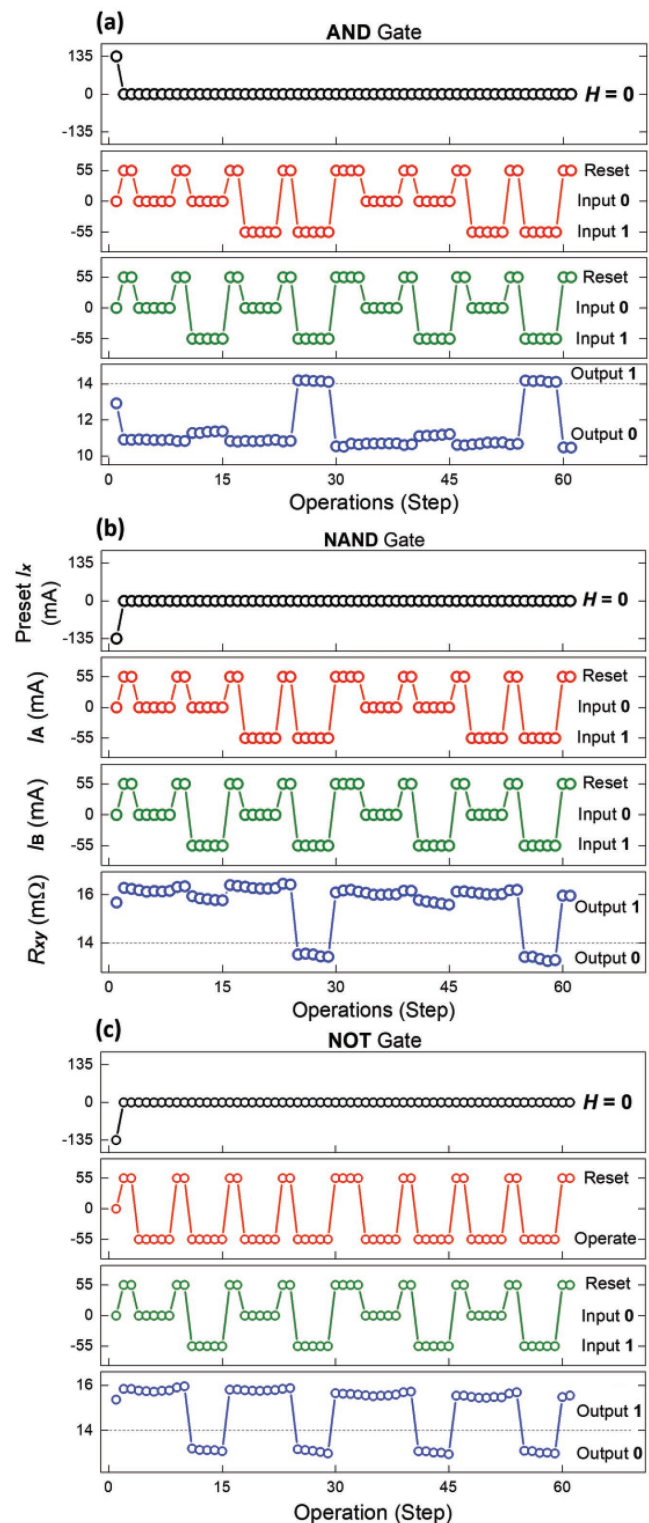


**Figure 3.** Programmable logic operations of a single device. Boolean functions of: a) AND, b) NAND, and c) NOT were realized. Preset  $I_x$  reconfigured the device among the different logic gates by a single pulse at the beginning of logic operations.  $I_A$  and  $I_B$  served as inputs. Output 0 and 1 was noticeably resolved by  $R_{xy}$ .  $R_{xy} \geq 14$  m $\Omega$  ( $R_{xy} < 14$  m $\Omega$ ) corresponded to Output 1 (0), respectively, as shown by dashed lines. AND and NAND gates were repeated two times and NOT gate was repeated four times.

$A = B = 0$  or  $I_A = I_B = 0$  mA, the perpendicular layer retained its initial spin-down state and the device output Logic 0. If either of Input  $A$  or  $B$  was chosen as 1, for example,  $I_A = -55$  mA and  $I_B = 0$  mA,  $|I_A + I_B|$  was still smaller than  $I_C$ , so the device also output Logic 0. Only when  $A = B = 1$  or  $I_A = I_B = -55$  mA and  $|I_A + I_B| > I_C$ , the perpendicular layer could be deterministically switched from the initial spin-down state to spin-up state, and then the output of device showed Logic 1. In this case, the device functioned as an AND gate (Figure 3a).

For NAND gate (Figure 3b),  $I_x = -135$  mA was first applied to reverse the SOT-switching chirality of the perpendicular layer from clockwise to counterclockwise by electrically switching the in-plane layer from  $m_y^{\text{top}} > 0$  to  $m_y^{\text{top}} < 0$ . This operation could mimic the function of an inverter and further enable our device to be programmable from the previous AND to the current NAND gate. Therefore, the same reset and logic operations as AND gate (shown by the same operations of  $I_A$  and  $I_B$  in Figure 3a,b) resulted in opposite logic outputs. The programmability between NAND and AND gates was nontrivial. It was the preset current  $I_x$  or SOT-switching of the in-plane layer that made the programmability come true.

For the NOT gate (Figure 3c), the preset and reset process was the same as the NAND gate. In logic operation process, only  $A$  was used as the input while  $B$  was fixed to  $-55$  mA. During the logic operations,  $A = 1$  (0) favored spin-down (spin-up) state and thus finally output 0 (1).

An ideal spin logic cell would better be based on a magnetic tunnel junction to improve the read margin. Then one side of the perpendicular layer has to be exposed to a barrier while the other side contacts a heavy metal providing SOT and mediating IEC, such as CoFeB/Ta/CoFeB/MgO/pinned layer. Though in perpendicularly coupled CoFeB/Ta/CoFeB systems, Shi<sup>[34]</sup> and Bi<sup>[35]</sup> have investigated the interplay of SOT and IEC, indicating possibility of transferring our technique into a CoFeB/Ta/CoFeB system with the crossed anisotropy. Besides, spin dynamics of Pt/Co/Ru/Co/Pt system driven by SOT shared similarity with the ideal CoFeB/Ta/CoFeB system if the thickness of the top and bottom Pt layers was fixed the same. In these systems, spin dynamics of the perpendicular and in-plane layers need to be both taken into account and utilize them in order to realize bilayer switching. (Theoretical analysis could be found in Section SC, Supporting Information.) It is a pronounced difference from the previous studies<sup>[20–24]</sup> where only dynamics of a perpendicular layer was considered. Furthermore, the field-like torque in the Pt/Co/Ru/Co/Pt system obtained in the second harmonic Hall measurement was very small and could be ignored (Section SB, Supporting Information), which made Pt/Co/Ru/Co/Pt system an ideal toy model to study switching mechanism driven purely by damping-like SOT in this crossed anisotropic system. This is the reason why the Pt/Co/Ru/Co/Pt system was chosen. While we cannot totally exclude the contribution from the spin current generated by in-plane ferromagnetic layer proposed by refs. [36,37], we have confirmed through second harmonic technique that the spin torques sensed by the perpendicular Co layer are mainly contributed by spin Hall effect of the Pt layers in our case (Section SB, Supporting Information). It is also worth pointing out that the coupling type, antiferromagnetic or ferromagnetic coupling between the two Co layers, is optional

for the chirality control and logic operations. Both of them can lead to similar results.

Spin logic based on magnetic tunnel junctions has charming advantages of nonvolatility, high speed, high parallel computing capability, and compatibility with current CMOS and magnetic random access memory technologies, being a promising way to achieve logic-in-memory architectures. However, its development is still hampered by the following issues such as lack of proper physical mechanisms to support fast and energy-efficient spin logic operations and demand of new cascading methods to realize compatibility of logic devices with emerging nonvolatile memories. Some pioneering studies<sup>[38,39]</sup> have already been devoted to the second issue and shown that non-volatile devices integrated into traditional CMOS circuits could be practical cascading solutions. Here, our results showed the magnetic bilayer system with crossed anisotropy could be fully controllable by pure electrical manners via the spin Hall effect without any aid of applied magnetic field. Controllable parameters included not only magnetizations of the films with in-plane and perpendicular anisotropy but also switching chirality of the perpendicular layer. These merits would make the crossed anisotropic system suitable to realize multistate memories and even logic-in-memory architectures in the future.

## Experimental Section

The stacks (Figure 1b,c, insets) were deposited on Si/SiO<sub>2</sub> substrates by magnetron sputtering technique (TMR R&D Sputtering System, ULVAC) with base pressure of  $1.0 \times 10^{-6}$  Pa at room temperature. During deposition process, an in-plane magnetic field to induce easy axis was provided. The stacks were then patterned via ultraviolet lithography and argon ion etching into two types of Hall bars with widths of 10 and 20  $\mu\text{m}$  as illustrated in Figures 1a and 3d, respectively. Cu/Au electrodes were finally deposited to connect terminals of the Hall bars. Magnetic properties were measured by vibrating sample magnetometer (VSM, Micro Sense) while magnetotransport properties such as Hall resistance  $R_{xy}$  were measured by four-terminal method. Keithley 2400 provided constant current  $I_x$  or  $I_y$  while Keithley 2182 picked up Hall voltages  $V_y$  or  $V_x$ . In the magnetotransport measurement, the magnetic field was provided by a Physical Property Measurement System (PPMS-9T, Quantum Design) or core-free Helmholtz coils. The latter could provide magnetic field of  $\pm 340$  Oe with negligible remanence ( $< 0.5$  Oe). Field-free switching performance was double-checked by taking samples fully out from magnet to avoid any remanence. Spin-orbit torques have been calibrated by standard second harmonic techniques as used in refs. [40,41] All the measurements were conducted at room temperature.

## Supporting Information

Supporting Information is available from the Wiley Online Library or from the author.

## Acknowledgements

X.W. and C.W. contributed equally to this work. This work was supported by the National Key Research and Development Program of China (MOST) (Grant No. 2017YFA0206200), the National Key Scientific Instrument and Equipment Development Projects (MOST) (Grant No. 2011YQ120053), the National Natural Science Foundation of China (NSFC) (Grant Nos. 11434014, 51701203, and 51620105004),

and partially supported by the Strategic Priority Research Program (B) (Grant No. XDB07030200), the Key Research Program of Frontier Sciences (Grant No. QYZDJ-SSW-SLH016), and the International Partnership Program (No. 112111KYSB20170090) of the Chinese Academy of Sciences (CAS). X.F.H. led and was involved in all aspects of the project. X.F.H. and C.W. supervised and designed the whole research. X.W. and L.H. deposited stacks. W.K., X.Z., and C.F. fabricated micro- and nanosized Hall devices. X.W., W.Y., and H.W. conducted magnetic property measurement. X.W., C.W., Y.X., and B.T. conducted switching and logic operations. C.W., X.W., and X.F.H. contributed to macro-spin modeling and wrote the paper. All the authors contributed to data mining and analysis.

## Conflict of Interest

The authors declare no conflict of interest.

## Keywords

interlayer exchange coupling, spin logic, spin-orbit torques, switching modes

Received: February 27, 2018

Revised: May 15, 2018

Published online: June 21, 2018

- [1] J. Wunderlich, B. G. Park, A. C. Irvine, L. P. Zárbo, E. Rozkotová, P. Nemeč, V. Novák, J. Sinova, T. Jungwirth, *Science* **2010**, *330*, 51801.
- [2] D. Bhowmik, L. You, S. Salahuddin, *Nat. Nanotechnol.* **2014**, *9*, 59.
- [3] D. E. Nikonova, I. A. Young, *J. Mater. Res.* **2014**, *29*, 2109.
- [4] S. Matsunaga, J. Hayakawa, S. Ikeda, K. Miura, H. Hasegawa, T. Endoh, H. Ohno, T. Hanyu, *Appl. Phys. Express* **2008**, *1*, 091301.
- [5] H. Lee, F. Ebrahimi, P. K. Amiri, K. L. Wang, *IEEE Magn. Lett.* **2016**, *7*, 3102505.
- [6] I. M. Miron, K. Garello, G. Gaudin, P.-J. Zermatten, M. V. Costache, S. Auffret, S. Bandiera, B. Rodmacq, A. Schuhl, P. Gambardella, *Nature* **2011**, *476*, 189.
- [7] L. Q. Liu, O. J. Lee, T. J. Gudmundsen, D. C. Ralph, R. A. Buhrman, *Phys. Rev. Lett.* **2012**, *109*, 096602.
- [8] M. M. Decker, M. S. Wörnle, A. Meisinger, M. Vogel, H. S. Körner, G. Y. Shi, C. Song, M. Kronseder, C. H. Back, *Phys. Rev. Lett.* **2017**, *118*, 257201.
- [9] R. Mishra, J. W. Yu, X. P. Qiu, M. Motapothula, T. Venkatesan, H. Yang, *Phys. Rev. Lett.* **2017**, *118*, 167201.
- [10] J. H. Han, A. Richardella, S. A. Siddiqui, J. Finley, N. Samarth, L. Q. Liu, *Phys. Rev. Lett.* **2017**, *119*, 077702.
- [11] K. Yasuda, A. Tsukazaki, R. Yoshimi, K. Kondou, K. S. Takahashi, Y. Otani, M. Kawasaki, Y. Tokura, *Phys. Rev. Lett.* **2017**, *119*, 137204.
- [12] C. H. Wan, X. Zhang, Z. H. Yuan, C. Fang, W. J. Kong, Q. T. Zhang, H. Wu, U. Khan, X. F. Han, *Adv. Electron. Mater.* **2017**, *3*, 1600282.
- [13] X. Zhang, C. H. Wan, Z. H. Yuan, C. Fang, W. J. Kong, H. Wu, Q. T. Zhang, B. S. Tao, X. F. Han, *J. Magn. Magn. Mater.* **2017**, *428*, 401.
- [14] S. Fukami, T. Anekawa, C. L. Zhang, H. Ohno, *Nat. Nanotechnol.* **2016**, *11*, 621.
- [15] X. Zhang, C. H. Wan, Z. H. Yuan, Q. T. Zhang, H. Wu, L. Huang, W. J. Kong, C. Fang, U. Khan, X. F. Han, *Phys. Rev. B* **2016**, *94*, 174434.
- [16] G. Q. Yu, P. Upadhyaya, Y. B. Fan, J. G. Alzate, W. J. Jiang, K. L. Wong, S. Takei, S. A. Bender, L. T. Chang, Y. Jiang, M. R. Lang, J. S. Tang, Y. Wang, Y. Tserkovnyak, P. K. Amiri, K. L. Wang, *Nat. Nanotechnol.* **2014**, *9*, 548.
- [17] L. You, O. Lee, D. Bhowmik, D. Labanowski, J. Hong, J. Bokor, S. Salahuddin, *Proc. Natl. Acad. Sci. USA* **2015**, *112*, 10310.
- [18] C. F. Pai, M. Mann, A. J. Tan, G. S. D. Beach, *Phys. Rev. B* **2016**, *93*, 144409.
- [19] V. M. Parakkat, K. R. Ganesh, P. S. A. Kumar, *Phys. Rev. B* **2017**, *96*, 104412.
- [20] S. Fukami, C. L. Zhang, S. D. Gupta, A. Kurenkov, H. Ohno, *Nat. Mater.* **2016**, *15*, 535.
- [21] A. Brink, G. Vermijs, A. Solignac, J. Koo, J. T. Kohlhepp, H. J. M. Swagten, B. Koopmans, *Nat. Commun.* **2016**, *7*, 10854.
- [22] Y. W. Oh, S. C. Baek, Y. M. Kim, H. Y. Lee, K. D. Lee, C. G. Yang, E. S. Park, K. S. Lee, K. W. Kim, G. Go, J. R. Jeong, B. C. Min, H. W. Lee, K. J. Lee, B. G. Park, *Nat. Nanotechnol.* **2016**, *11*, 878.
- [23] Y. C. Lau, D. Betto, K. Rode, J. M. D. Coey, P. Stamenov, *Nat. Nanotechnol.* **2016**, *11*, 758.
- [24] W. J. Kong, Y. R. Ji, X. Zhang, H. Wu, Q. T. Zhang, Z. H. Yuan, C. H. Wan, X. F. Han, T. Yu, K. Fukuda, H. Naganuma, M. J. Tung, *Appl. Phys. Lett.* **2016**, *109*, 132402.
- [25] A. Kurenkov, C. Zhang, S. DuttaGupta, S. Fukami, H. Ohno, *Appl. Phys. Lett.* **2017**, *110*, 092410.
- [26] J. Y. Chen, D. C. Mahendra, D. L. Zhang, Z. Y. Zhao, M. Li, J. P. Wang, *Appl. Phys. Lett.* **2017**, *111*, 012402.
- [27] K. M. Cai, M. Y. Yang, H. L. Ju, S. M. Wang, Y. Ji, B. H. Li, K. W. Edmonds, Y. Sheng, B. Zhang, N. Zhang, S. Liu, H. Z. Zheng, K. Y. Wang, *Nat. Mater.* **2017**, *16*, 712.
- [28] X. P. Qiu, K. Narayanapillai, Y. Wu, P. Deorani, D. H. Yang, W. S. Noh, J. H. Park, K. J. Lee, H. W. Lee, H. Yang, *Nat. Nanotechnol.* **2015**, *10*, 333.
- [29] L. Q. Liu, C. F. Pai, Y. Li, H. W. Tseng, D. C. Ralph, R. A. Buhrman, *Science* **2012**, *336*, 555.
- [30] G. E. Rowlands, S. V. Aradhya, S. Shi, E. H. Yandel, J. Oh, D. C. Ralph, R. A. Buhrman, *Appl. Phys. Lett.* **2017**, *110*, 122402.
- [31] X. Wang, L. Huang, Y. Zhu, Y. Zhou, H. Peng, H. Xiong, in *IEEE 17th Int. Conf. High Performance Computing and Communications (HPCC)*, IEEE, Piscataway, NJ, USA **2015**.
- [32] M. Qiu, Z. Chen, Z. Ming, X. Qin, J. Niu, *IEEE Syst. J.* **2017**, *11*, 813.
- [33] A. Ney, C. Pampuch, R. Koch, K. H. Ploog, *Nature* **2003**, *425*, 485.
- [34] G. Y. Shi, C. H. Wan, Y. S. Chang, F. Li, X. J. Zhou, P. X. Zhang, J. W. Cai, X. F. Han, F. Pan, C. Song, *Phys. Rev. B* **2017**, *95*, 104435.
- [35] C. Bi, H. Almasi, K. Price, T. Newhouse-Illice, M. Xu, S. R. Allen, X. Fan, W. G. Wang, *Phys. Rev. B* **2017**, *95*, 104434.
- [36] A. M. Humphries, T. Wang, E. R. J. Edwards, S. R. Allen, J. M. Shaw, H. T. Nembach, J. Q. Xiao, T. J. Silva, X. Fan, *Nat. Commun.* **2017**, *8*, 911.
- [37] S. C. Baek, V. P. Amin, Y. W. Oh, G. Go, S. J. Lee, G. H. Lee, K. J. Kim, M. D. Stiles, B. G. Park, K. J. Lee, *Nat. Mater.* **2018**, *17*, 509.
- [38] Y. J. Zhang, B. Yan, W. Wu, H. Li, Y. Chen, presented at *2015 Design, Automation and Test in Europe Conf. Exhibition (DATE)*, Grenoble, France, March **2015**.
- [39] S. Matsunaga, J. Hayakawa, S. Ikeda, K. Miura, H. Hasegawa, T. Endoh, H. Ohno, T. Hanyu, *Appl. Phys. Express* **2008**, *1*, 091301.
- [40] U. H. Pi, K. W. Kim, J. Y. Bae, S. C. Lee, Y. J. Cho, K. S. Kim, S. Seo, *Appl. Phys. Lett.* **2010**, *97*, 162507.
- [41] J. Kim, J. Sinha, M. Hayashi, M. Yamanouchi, S. Fukami, T. Suzuki, S. Mitani, H. Ohno, *Nat. Mater.* **2012**, *12*, 240.